Langmuir
Article
pubs.acs.org/Langmuir

Seeded Growth of Titania Colloids with Refractive Index Tunability and Fluorophore-Free Luminescence

Ahmet Faik Demirörs,*[,†] Anita Jannasch,[‡] Peter D. J. van Oostrum,[†] Erik Schäffer,[‡] Arnout Imhof,[†] and Alfons van Blaaderen*[,†]

[†]*Soft Condensed Matter, Debye Institute for Nanomaterials Science, Department of Physics and Astronomy, Utrecht University, Princetonplein 5, 3584 CC Utrecht, The Netherlands, and* [‡]*Nanomechanics Group, Biotechnology Center, TU Dresden, Tatzberg 47-51, 01307 Dresden, Germany*

Received September 16, 2010. Revised Manuscript Received December 10, 2010

Titania is an important material in modern materials science, chemistry, and physics because of its special catalytic, electric, and optical properties. Here, we describe a novel method to synthesize colloidal particles with a crystalline titania, anatase core and an amorphous titania-shell structure. We demonstrate seeded growth of titania onto titania particles with accurate particle size tunability. The monodispersity is improved to such an extent so that colloidal crystallization of the grown microspheres becomes feasible. Furthermore, seeded growth provides separate manipulation of the core and shell. We tuned the refractive index of the amorphous shell between 1.55 and 2.3. In addition, the particles show luminescence when trace amounts of aminopropyl-triethoxysilane are incorporated into the titania matrix and are calcined at 450 °C. Our novel colloids may be useful for optical materials and technologies such as photonic crystals and optical trapping.

1. Introduction

Titania is abundantly studied in the literature for its importance in many fields such as catalysis (both as a catalyst[1] and as a support[2]), in Grätzel-type solar cells as a semiconductor for conversion of light to electricity,[3] in colloidal photonic crystals, and as a paint pigment for its high refractive index.[4−6] Although there was scientific demand for colloidal titania in many areas, fast reaction kinetics of the titania precursors made the synthesis of highly monodisperse titania colloids difficult to achieve in a reproducible manner, until recently. Barringer and Bowen[7] and Jean and Ring[8] reported synthesis procedures for monodisperse titania, but their methods were not easily reproducible. Additionally there were approaches with aerosol[9] and hydrolysis[10] techniques; however, they had redispersing difficulties together with aggregation and monodispersity. Recently, Eiden-Assman et al.,[11] Yu et al.,[12] and Jiang et al.[13] succeeded in producing monodisperse titania particles, with a procedure that we were able to reproduce. Also, after calcination the latter methods gave more spherical colloids with respect to the method of Barringer et al. and Jean et al.[14] All methods referred make use of the hydrolysis of titanium alkoxides and control their precipitation using a (nonionic) surfactant. The method of Eiden-Assman is notable for its high particle yield compared to other methods, and it is optimum for making particles of ∼1 μm in size, whereas the others give particles in the size range of 200−650 nm.

In previous work, we have developed a general method with which a layer of amorphous titania can be grown on many different colloids.[15] We have also shown that the pore structure of this titania is accessible to other chemicals such as dyes and silica, which can be used to modify it.[16,17] These methods also apply to the coating of titania itself, that is, seeded growth. But more importantly, this approach offers a way to tune the optical properties of titania−titania core−shell colloids, in particular the refractive index and luminescence.

Seeded growth—well-known for the growth of silica particles—is in general an attractive way to obtain fine control of particle growth, as it also helps to decrease the polydispersity of the particles.[18] In this article we show seeded growth of titania particles with amorphous titania starting from a crystalline titania core resulting in a core−shell structure with different refractive indices.

This core−shell structure opens the way to tailor the refractive index of the core independently from that of the shell, which makes our particles useful candidates for photonic crystal applications and optical trapping.[19,20] It was shown by Velikov et al.[21]

*To whom correspondence should be addressed. A.F. Demirörs: A.F. Demirors@uu.nl. A. van Blaaderen: A.vanBlaaderen@uu.nl.

(1) Hoffmann, M. R.; Martin, S. T.; Choi, W. Y.; Bahnemann, D. W. *Chem. Rev*. **1995**, *95*, 69–96.
(2) Valden, M.; Lai, X.; Goodman, D. W. *Science* **1998**, *281*, 1647–1650.
(3) Oregan, B.; Gratzel, M. *Nature* **1991**, *353*, 737–740.
(4) Imhof, A.; Pine, D. J. *Nature* **1997**, *389*, 948–951.
(5) Wijnhoven, J.; Vos, W. L. *Science* **1998**, *281*, 802–804.
(6) Lodahl, P.; van Driel, A. F.; Nikolaev, I. S.; Irman, A.; Overgaag, K.; Vanmaekelbergh, D. L.; Vos, W. L. *Nature* **2004**, *430*, 654–657.
(7) Barringer, E. A.; Bowen, H. K. *Langmuir* **1985**, *1*, 414–420.
(8) Jean, J. H.; Ring, T. A. *Langmuir* **1986**, *2*, 251–255.
(9) Spicer, P. T.; Chaoul, O.; Tsantilis, S.; Pratsinis, S. E. *J. Aerosol Sci*. **2002**, *33*, 17–34.
(10) Park, H. K.; Kim, D. K.; Kim, C. H. *J. Am. Ceram. Soc*. **1997**, *80*, 743–749.
(11) Eiden-Assmann, S.; Widoniak, J.; Maret, G. *Chem. Mater*. **2004**, *16*, 6–11.
(12) Yu, H. K.; Yi, G. R.; Kang, J. H.; Cho, Y. S.; Manoharan, V. N.; Pine, D. J.; Yang, S. M. *Chem. Mater*. **2008**, *20*, 2704–2710.
(13) Jiang, X. C.; Herricks, T.; Xia, Y. N. *Adv. Mater*. **2003**, *15*, 1205.
(14) Holgado, M.; Cintas, A.; Ibisate, M.; Serna, C. J.; Lopez, C.; Meseguer, F. *J. Colloid Interface Sci*. **2000**, *229*, 6–11.
(15) Demirörs, A. F.; van Blaaderen, A.; Imhof, A. *Langmuir* **2010**, *26*, 9297–9303.
(16) Demirörs, A. F.; van Blaaderen, A.; Imhof, A. *Chem. Mater*. **2009**, *21*, 979–984.
(17) Demirörs, A. F.; Imhof, A. *Chem. Mater*. **2009**, *21*, 3002–3007.
(18) van Blaaderen, A.; van Geest, J.; Vrij, A. *J. Colloid Interface Sci*. **1992**, *154*, 481–501.
(19) Bormuth, V.; Jannasch, A.; Ander, M.; van Kats, C. M.; van Blaaderen, A.; Howard, J.; Schaffer, E. *Opt. Express* **2008**, *16*, 13831–13844.
(20) Jannasch, A.; Bormuth, V.; van Kats, C. M.; van Blaaderen, A.; Howard, J.; Schaffer, E. Art. no. 703821B. In *Optical Trapping and Optical Micromanipulation V*; Dholakia, K., Spalding, G. C., Eds.; Spie-Int Soc. Optical Engineering: Bellingham, 2008; Vol. *7038*, pp B3821−B3821.

Scheme 1. Schematic Representation of the Procedure for Fabrication of Core−Shell Titania Structures[a]

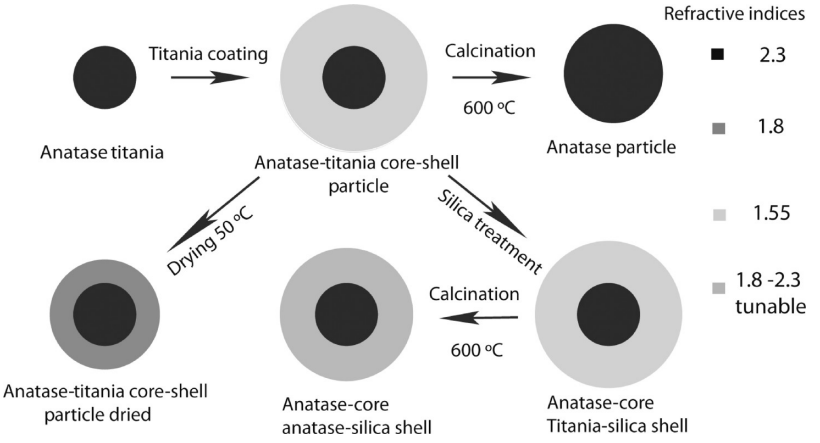

[a] Note that all particles have a crystalline−titania (anatase) core. The particles are coated with amorphous titania and manipulated by heating and silica treatments.

that the L-stopgap width in *fcc* photonic crystals of high-index core and low-index shell particles was larger in comparison to the case of homogeneous particles of either material. It was also shown that a core−shell morphology could give additional control over the photonic stopgap characteristics like bandwidth, position, and depth of the stopgap.[21] Moreover, monodisperse microspheres with tunable refractive index have potential applications as microlenses,[22] light scatterers, and diffusers[23] and as optical resonators.[24,25] Here we present a method by which the refractive index of the shell can be tuned from 1.55 to 2.3 using silica incorporation and calcination steps. This yields structures with an anatase core and titania-silica shell.

In addition to the above-mentioned applications, the luminescence of titania has attracted attention in the literature. Anatase is luminescent itself; however, the luminescence of anatase is significant only at ultralow temperatures, and the intensity is much reduced at room temperature.[26] Room temperature luminescence reports of titania mostly include incorporation of a dye,[3] a luminescent lanthanide,[27] or quantum dots[28,29] into the matrix. Here, we demonstrate that titania can be made luminescent in the visible by incorporating trace amounts of aminopropyl-triethoxysilane (APS) into the titania matrix and calcination at 450 °C. This is a fluorophore-free method where luminescence is caused by the residues left by of calcination of APS.[30,31]

2. Experimental Details

A schematic representation of the procedure for fabrication of core−shell titania structures is given in Scheme 1. It is shown here that starting from a crystalline titania-core one can make various core−shell particles with different refractive indices of the shell ranging from 1.55 to 2.3. Heating steps cause shrinkage of amorphous titania. Calcination of the core−shell particle yields fully crystalline titania particles with a larger size, whereas silica incorporation of these particles limits shrinkage and keeps the density and refractive index low. The refractive index of the final silica−titania shell depends on the amount of silica incorporated and the calcination time and temperature. Note that the amount of shrinkage, the final porosity, that is, the density, and the amount of titania filling are intrinsically linked. This means that we did not tune these parameters independently from each other in addition to varying the refractive index.

Crystalline titania cores were synthesized according to the procedure of Yu et al. with slight modifications.[12] For the synthesis, two solutions were prepared. The first was a 0.46% (w/w) titanium butoxide (TBT) (97%, Aldrich) solution in ethylene glycol, which also chelates with titanium. The second was an acetone solution of the surfactant Tween 20 (274348, Sigma-Aldrich, average M_n ~1228) with a Tween 20 concentration of 2.03 mM. Acetone used for Tween 20 solution was reagent grade (99.7%), and for a 100 mL of acetone ~100 μL of water was added. Note that this small amount of water added in acetone turned out to be crucial for realizing a successful spherical and monodisperse particle synthesis. A portion of 10−20 mL of the TBT solution was mixed with 100 mL of the acetone−Tween 20 mixture and agitated for a few minutes. The transparent solution became milky white after 10 min, and the white precipitate was collected by centrifugation the next day. With this technique it was possible to synthesize anatase−titania particles in the 200−650 nm range after calcination at 500 °C for 1 h. A portion of 14 mL of TBT solution in 100 mL of acetone solution gave the 450 nm particles used in this work.

The anatase core particles obtained after calcination were dispersed in ethanol by sonication. A portion of 80 μL of 0.1 M aqueous Lutensol ON50 (BASF) solution was added to a 10 mL dispersion of 1.4−2.4 mg core particles. In another 10 mL of ethanol, 0.1−0.2 mL of TBT was added, and the diluted titania precursor was mixed with the core particle dispersion.[11,15] The mixture was sonicated for at least 20 min in a sonication bath during the reaction. This gave monodisperse titania core−shell particles with a total size between 700 and 1100 nm depending on the amount of the titania precursor used and on the seed particle concentration. The titania particles were collected by centrifugation and then dispersed in fresh ethanol without drying. The ethanol used in this work (for the synthesis) was analytical grade and at least 99.7% pure. Also, it was kept in the refrigerator at around 7 °C prior to use. Note also that seeded growth of amorphous titania particles was also possible, but we focused on anatase cores here (see Supporting Information, Figure S1).

(21) Velikov, K. P.; Moroz, A.; van Blaaderen, A. *Appl. Phys. Lett.* **2002**, *80*, 49–51.
(22) Serpe, M. J.; Kim, J.; Lyon, L. A. *Adv. Mater.* **2004**, *16*, 184.
(23) Goldenberg, J. F.; McKechnie, T. S. *J. Opt. Soc. Am. A* **1985**, *2*, 2337–2348.
(24) Spillane, S. M.; Kippenberg, T. J.; Vahala, K. J. *Nature* **2002**, *415*, 621–623.
(25) Gomez, D. E.; Pastoriza-Santos, I.; Mulvaney, P. *Small* **2005**, *1*, 238–241.
(26) Tang, H.; Berger, H.; Schmid, P. E.; Levy, F. *Solid State Commun.* **1994**, *92*, 267–271.
(27) Frindell, K. L.; Bartl, M. H.; Popitsch, A.; Stucky, G. D. *Angew. Chem. Int. Ed.* **2002**, *41*, 959.
(28) Robel, I.; Subramanian, V.; Kuno, M.; Kamat, P. V. *J. Am. Chem. Soc.* **2006**, *128*, 2385–2393.
(29) Zaban, A.; Micic, O. I.; Gregg, B. A.; Nozik, A. J. *Langmuir* **1998**, *14*, 3153−3156, doi: 10.1021/la9713863.
(30) Jakob, A. M.; Schmedake, T. A. *Chem. Mater.* **2006**, *18*, 3173–3175.
(31) Wang, L.; Estevez, M. C.; O'Donoghue, M.; Tan, W. H. *Langmuir* **2008**, *24*, 1635–1639.

Silica incorporation in the amorphous titania shell was performed according to the procedure for composite particles described in previous work,[16] which basically involved silica synthesis under Stöber conditions in the presence of the anatase-titania core−shell particles. For the silica incorporation 1.5 mg anatase seeds were grown with 0.15 mL of TBT in 20 mL of ethanol, and after the centrifugation of the grown particles these particles were dispersed in 10 mL of fresh ethanol without drying. A portion of 200 μL of tetraethyl orthosilicate (TEOS) was then added to the dispersion of particles along with 0.2 mL of concentrated ammonia (30% in water, Sigma-Aldrich) for the particles the scattering of which is depicted in Figure 4a. Similar syntheses with 0.14 mL of TBT yielded the particles given in Figure 4b(1), after incorporation of 100 μL of TEOS to the shell and calcination at 500 °C for 1 h. The particles in Figure 4b(2) were produced similarly to the ones in Figure 4b(1) with a decrease to 50 μL of TEOS. In another synthesis, 2.3 mg of anatase seeds were coated with titania in a total of 30 mL by addition of 0.2 mL of TBT. Particles in this batch were divided into three. All three batches were dispersed in 10 mL of ethanol, followed by addition of 0.1 mL of ammonia and 0.5, 2, and 10 μL of APS, respectively. The 0.5 μL of APS batch was calcined at 400 °C, and the others were calcined at 450 °C for 2 h. The latter two particles are shown in Figure 4c(1) and (2).

Methods. *Confocal Microscopy*. For confocal microscopy measurements (inverted Nikon EZ-C1 with a 63 × 1.4 NA oil immersion objective), the fluorescent dye rhodamine isothiocyanate (RITC) was added to the dispersion of the particles that absorbed part of the dye, and the particles were centrifuged afterward to remove excess dye. For the particles that were made to luminesce due to incorporation of APS and calcination, a 488 nm laser was used for excitation, and the detector slit was selected to be between 590 and 620 nm.

Static Light Scattering (*SLS*). Static light scattering was performed with home-built equipment using a He−Ne laser as a light source (632.8 nm, 10 mW). The logarithm of scattering intensity data was plotted against the scattering vector $k = 4\pi n \sin(\theta/2)/\lambda$, where n is the solvent refractive index, θ is the scattering angle, and λ is the wavelength in vacuum.

Fluorescence Spectroscopy. Emission spectra were measured with a SPEX DM3000F spectrofluorometer with a 450 W Xe lamp as the excitation source. Excitation and emission wavelengths were selected with a double-grating 0.220 m SPEX 1680 monochromator (1200 L/mm) blazed at 300 nm. Emission spectra were recorded by focusing the emitted light on a fiber guiding the light to a 0.3 m Acton Research monochromator (Scientific Spectra Pro, Princeton Instruments). The dispersed light was detected with a Princeton Instruments 300i charge−coupled device. Measurements were performed using a quartz cuvette with a dilute dispersion of particles (approximately 0.5% (v/v)) in ethanol.

Transmission Electron Microscopy (*TEM*) *and Energy Dispersive X-ray Analysis*. Energy dispersive X-ray (EDX) analysis and transmission electron microscopy (TEM) images were obtained with a Philips Tecnai 12 or 20 electron microscope. Sizes of the particles were determined by analyzing at least 150 particles.

Digital Holographic Microscopy. Our holographic analysis instrument is based on a standard inverted optical microscope (Leica DMIRB), with a laser diode (Pegasus PE.P532, λ = 532 nm) replacing the conventional incandescent illuminator and condenser. Light scattered by a particle propagates to the microscope's focal plane, where it interferes with the undiffracted fraction of the beam.[32] The resulting interference pattern is magnified by the microscopes objective lens (Leica 100 × NA 1.4 oil immersion Plan-Apo) onto the sensor of a gray scale video camera (Mikrotron EoSens CL). This system provides a total magnification of 141.6 ± 1 nm/pixel over a 181 by 45 μm field of view.

(32) Sheng, J.; Malkiel, E.; Katz, J. *Appl. Opt*. **2006**, *45*, 3893–3901.

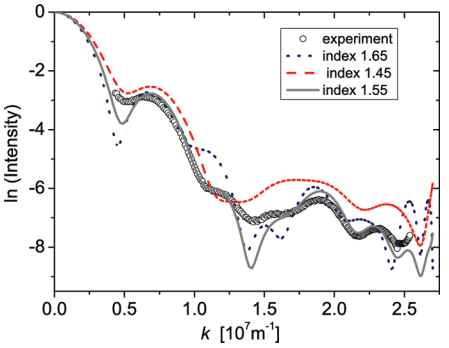

Figure 1. SLS experimental curves of the titania particles (symbols) in ethanol fitted to theoretical calculations of the full Mie solutions to the form factor (lines, offset for clarity). Dried core−shell particles given in Figure 2c and three different Mie solutions to the experimental data to give an idea about the accuracy of the refractive index assignment with SLS technique. The calculations with ±0.1 refractive index change differs a lot from the experimental curve and cannot match the minima. The calculations with ±0.05 (see Supporting Information, Figure S2) index change are still off from the minima but we preferred to show the ±0.1 change for better visualization (k = scattering vector).

Fitting these digitized holograms to a model that includes the analytic description of light scattering by Lorenz and Mie[33] yields the particles three-dimensional position, r, its radius, a, and its index of refraction, n.[34]

3. Results and Discussion

We performed a thorough SLS study of these particles; this method gives an easy way to estimate the size, polydispersity, and the refractive index. The locations of the minima and maxima as a function of the scattering vector (k-axis) depend sensitively on the particle size and refractive index, whereas the depth of the minima gives an estimate of the polydispersity. For the same material the number of minima increases with particle size.[34,35] The accuracy of the SLS to determine the refractive index (and size) is shown in Figure 1. The calculations with a ±0.1 refractive index change differ noticeably from the experimental curve and cannot match the locations of the minima. The calculations with ±0.05 (see Supporting Information, Figure S2) index difference are still off from the minima, but we preferred to show the ±0.1 change for better visualization. With a starting input of the size estimated by TEM, these measurements support the more exact determination of size and refractive index by SLS.

For some particles, the SLS measurements were performed in ethanol and in dimethyl sulfoxide (DMSO) as a solvent to have more features due to the different refractive index contrasts. This provides a better estimate of the parameters by comparing the data with each other. Figure 2 shows the SLS graphs of the titania particles. Symbols in the graphs are the experimental data; lines are Mie calculations for the form factor. Size estimates of the anatase seed particles, given in Figure 2a, agree for both ethanol (refractive index n = 1.36) and DMSO (n = 1.479) with a particle refractive index of 2.3. Here the size of the seed particles was found to be 450 nm with a 10% polydispersity, which agrees with the TEM data (Table 1). Note that for all core−shell particles this core size and refractive index was used in the calculations.

(33) Lee, S. H.; Roichman, Y.; Yi, G. R.; Kim, S. H.; Yang, S. M.; van Blaaderen, A.; van Oostrum, P.; Grier, D. G. *Opt. Express* **2007**, *15*, 18275–18282.
(34) Bohren, C. F.; Huffman, C. F. In *Absorption and Scattering of Light by Small Particles*; Wiley: New York, 1983.
(35) Kerker, M.; Smith, L. B.; Matijevic, E.; Farone, W. A. *J. Colloid Sci*. **1964**, *19*, 193.

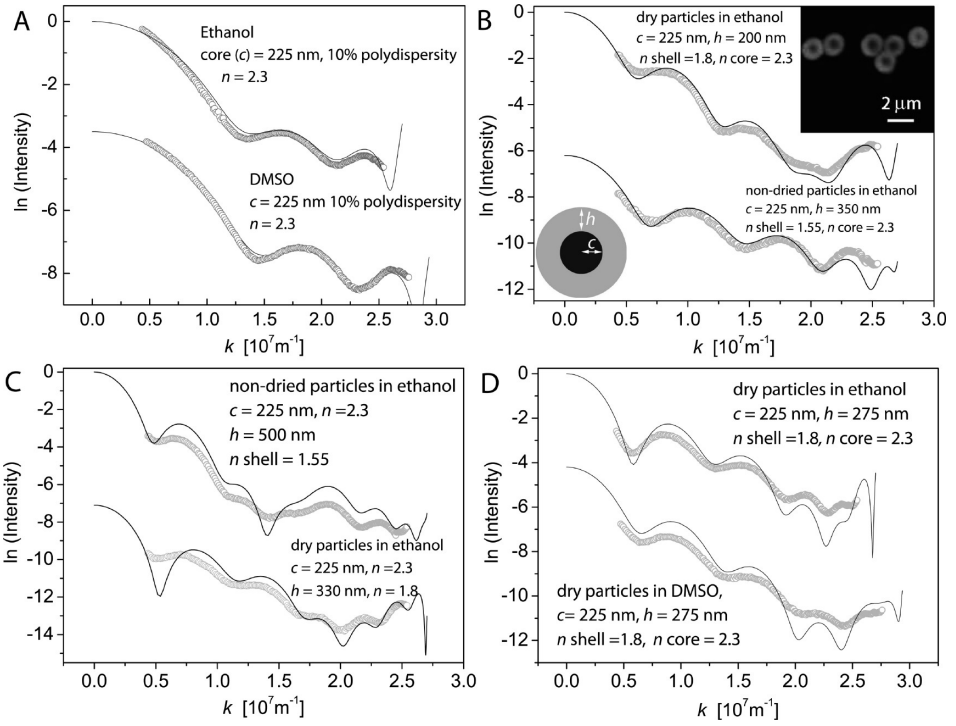

Figure 2. SLS experimental curves of the titania particles (symbols) in ethanol fitted to theoretical calculations of the full Mie solutions to the form factor (lines, offset for clarity). For the Mie solutions the polydispersity of the core was assumed to be 10%, and for all graphs the polydispersity for the shell was assumed to be 0%. Core radii (c), shell thicknesses (h), and refractive indices (n) are shown on the graphs and illustrated in the inset of Figure 2a. (a) Anatase core particles used as seed for growth, (b) core−shell particles prior to drying (350 nm shell) and after drying (200 nm shell) in ethanol; inset is the fluorescence microscopy image of as-synthesized anatase core, titania shell particles after addition of fluorescent dye, where dye can only reach the shell, (c) core−shell particles prior to drying (550 nm shell) and after drying (330 nm shell) in ethanol, and (d) core−shell particles after drying (275 nm shell) in ethanol and in DMSO (k = scattering vector).

Table 1. Total Diameter from TEM and SLS of the Particles Given in Figures *2* and *4*,[a]

particles (figure no.)	2a	2b	2c	2d	4a(1)	4a(2)	4c(1)	4c(2)
TEM size [nm]	440 (9%)	715 (4%)	903 (2%)	850 (3%)	675 (4%)	1047 (3%)	866 (4%)	885 (4%)
SLS size [nm]	450 (10%)	850 (5%)	1110 (4%)	1000 (4%)	710 (6%)	1030 (4%)	890 (4%)	910 (4%)

[a] Polydispersities of the particles are given in parentheses.

The literature value for the refractive index of anatase at 633 nm is 2.5.[36] However, the value we find is slightly lower, probably due to some remaining porosity. From X-ray diffraction analysis (data not shown) we know that the anatase core consists of nanocrystals with a typical size of 10 nm, which explains the lower index.

Core−shell particles fabricated by coating the anatase seeds with amorphous titania were examined by SLS before and after drying. It was observed that amorphous titania as-synthesized is highly porous, as was observed before, but densifies upon drying.[16] Thus, drying reduces the shell thickness but increases the refractive index and the density. This is confirmed in Figure 2 parts b and c, which show the SLS graphs for two examples of core−shell particles with unique features. In Figure 2b we found the thickness of the shell prior to drying to be 350 nm and a refractive index of 1.55. The shell thickness decreased to 200 nm upon drying, whereas the refractive index increased to 1.8. From Figure 2c the thickness of the shell prior to drying was determined to be 500 nm with a refractive index of 1.55. The shell thickness became 330 nm upon drying with a refractive index of 1.8. Another dried particle system that we examined in DMSO and in ethanol gave consistent results at these different index contrasts. The refractive index of the shell from both measurements was found to be 1.8 with a 275 nm shell thickness, as shown in Figure 2d. All of these analyses agree on a refractive index of 1.55 for nondried amorphous titania and a refractive index of 1.8 for dried and shrunken titania samples. Note that, in the core−shell morphologies the polydispersity for the shell (but not the core) was assumed to be 0%.

To reconfirm the results from SLS, we have also performed digital holographic microscopy (DHM) to measure the refractive index and size of individual titania particles.[33] This technique characterizes the particles by numerically solving the inverse problem posed by the analytical Lorenz−Mie[34] description for the scattering of single dielectrics and the in-line holograms.[32] We applied DHM to amorphous, dried, and calcined titania particles of the same original batch. The size and refractive indices of these particles were determined by SLS and TEM to be 850, 580, and 490 nm in radius and 1.55, 1.8, and 2.2 in refractive index for amorphous, dried, and calcined titania particles, respectively. Figure 3 shows the normalized holograms, the fitted hologram, and the azimuthally averaged radial intensity profiles for particles after the different treatments.

Figure 3a shows a typical hologram, with the fit and the intensity profile for a nondried (amorphous) titania particle.

(36) Howard, C. J.; Sabine, T. M.; Dickson, F. *Acta Crystallogr., Sect. B* **1991**, *47*, 462–468.

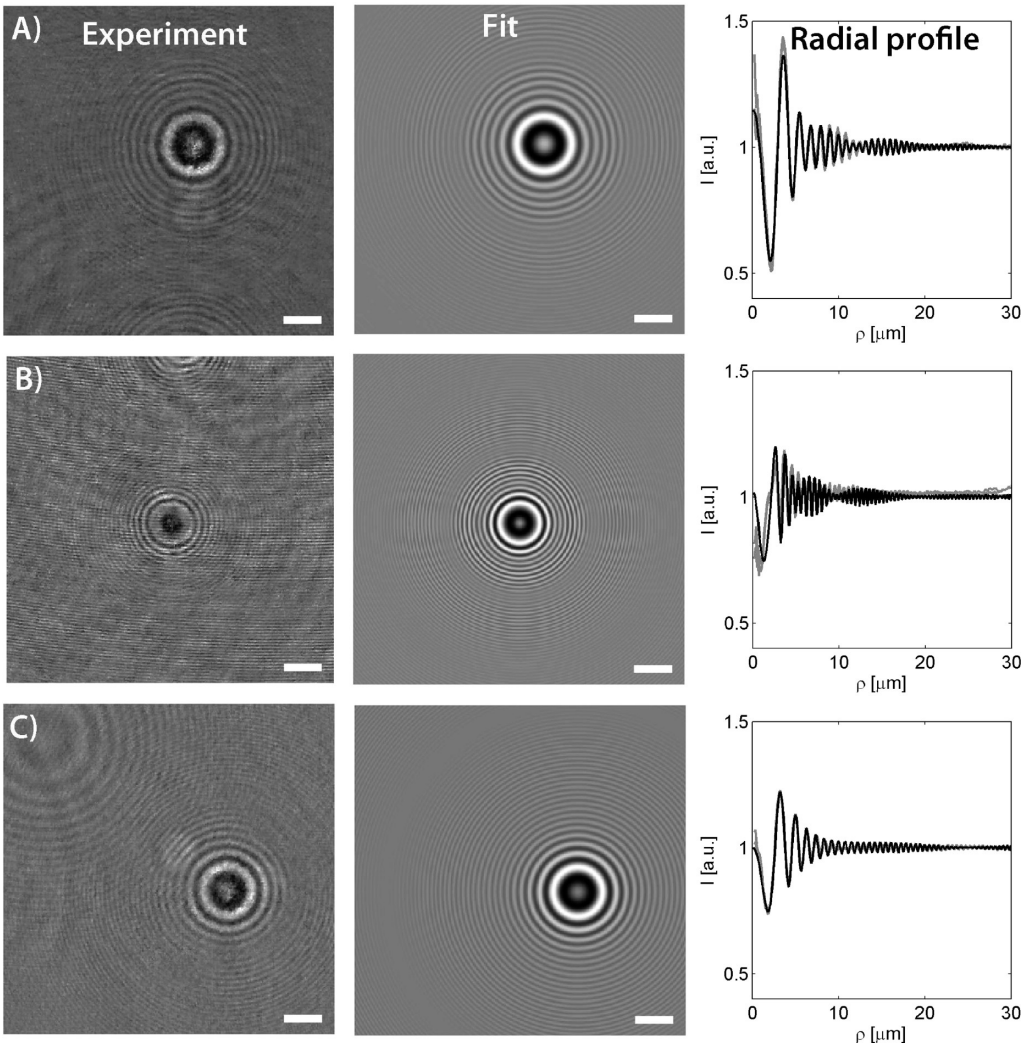

Figure 3. Normalized holograms, fitted holograms and azimuthally radial averages of the intensity of: (a) an amorphous titania particle of 902 nm in radius and with a refractive index of 1.55 at 22.82 μm depth, (b) a 666 nm radius dried titania particle with a refractive index of 1.87 at 8.85 μm above the focal plane and (c) a calcined titania particle at 450 °C with a radius of 553 nm and a refractive index of 2.2. The full lines in the intensity profiles are from the fit and the gray lines represent the experimental data ± 1 σ uncertainty levels. All scale bars are 5 μm.

The particle was found to be 22.82 μm above the focal plane of the microscope. The fit values for the radius and refractive index of this particle were 902 nm and 1.55, respectively. An example of a hologram of a particle after drying is presented in Figure 3b. The distance to the focal plane, the radius, and the refractive index were 8.85 μm, 666 nm, and 1.87, respectively. Finally, in Figure 3c, we include a hologram, its fit, and the corresponding intensity profile for a titania particle that was calcined at 450 °C. We measured the particle at a depth of 18.36 μm, with a radius of 553 nm, and a refractive index of 2.20. The general trend in the shrinkage and the rise in refractive index when the particles are subsequently dried and calcined from holography agrees with the SLS and TEM results (see Supporting Information, Figure S1 and Table S1). The observed particle sizes fall within the size distribution as determined by SLS. The fit values we obtained differed from particle to particle. Given the porous nature of the titania it is not surprising that we find different values for individual particles.

TEM analysis for crystalline particles gave similar sizes to the SLS curves (Table 1). TEM analysis data and the SLS data deviate for amorphous titania particles, which we attribute to a further shrinkage of the amorphous titania in the TEM as an effect of drying under high vacuum and heating by the electron beam. Note that the shrinkage of these particles under the influence of the electron beam was indeed observed during TEM experimentation. In Table 1, a decrease in the polydispersity is also observed with the particle growth. The 10% polydispersity of the core has decreased down to 3−4% values as the particles have grown to a 1 μm size.

To manipulate the refractive index of the shell to a higher precision we used a trick that was demonstrated previously,[16] where silica−titania composite particles were produced using nondried titania. The porosity of the as-synthesized titania makes it accessible for hydrolyzed silica precursors to condense inside the pores. Thus, the amount of incorporated silica determines the composition, refractive index, and density of the final product.

It is expected that the addition of silica, which is a low refractive index material, will decrease the refractive index of the shell and may also prevent shell shrinkage by filling the pores in the titania shell. This is shown by the example of anatase core particles with a titania−silica composite shell given in Figure 4a (curve 2). The refractive index for the composite shell after drying was indeed found to be 1.55 from the SLS curve. This agrees with our prediction, as the refractive index of the shell would have been 1.8

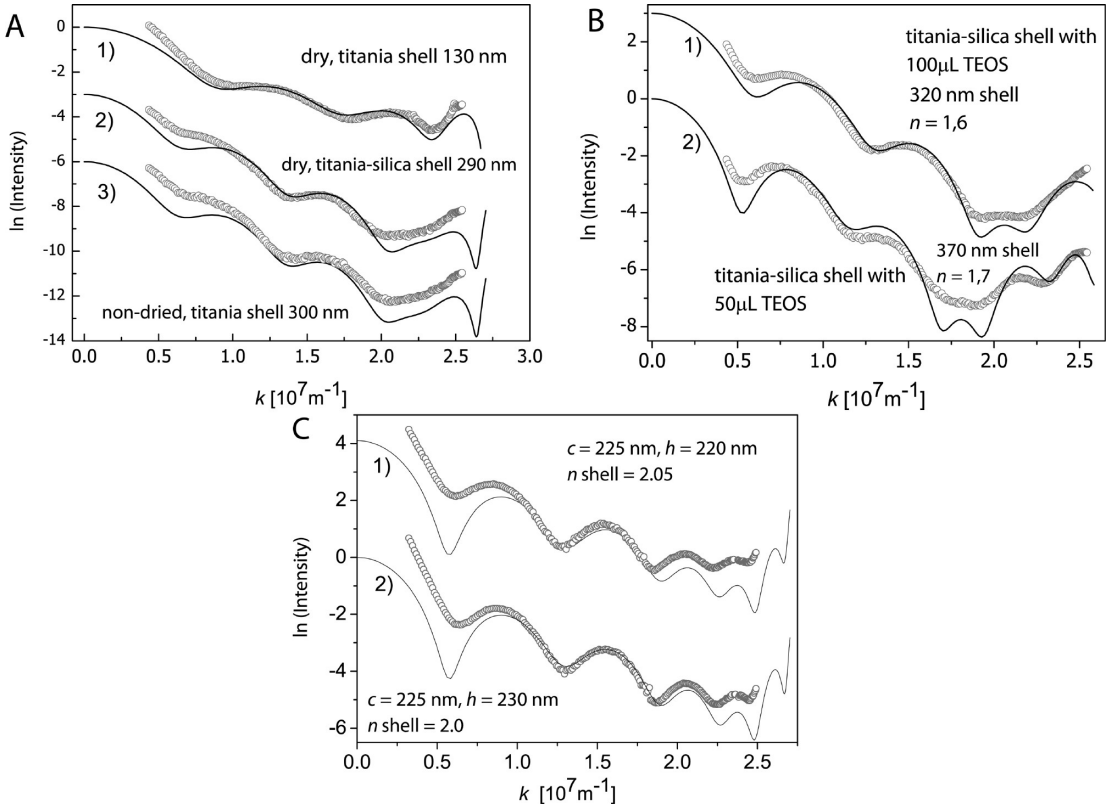

Figure 4. SLS graphs, (a) core−shell particles (1) after drying with titania-only shell (130 nm shell), (2) core−shell particles with silica incorporated into the titania shell with a thickness of 290 nm size after drying, (3) the same particles prior to drying and without the silica incorporation, only titania shell of 300 nm size. (b) Core−shell particles treated with silica (with composite shells) and calcined at 500 °C for 1 h. The shell refractive index in (1) is 1.6 with a shell thickness of 320 nm, and in (2) it is 1.7 with a 370 nm thick shell. (c) Similarly produced core−shell particles with lower silica content upon calcination 2 h at 450 °C. The shell refractive index in (1) is 2.05 with a shell thickness of 220 nm, and in (2) it is 2.0 with a 230 nm thick shell. All particles in (a), (b), and (c) have the same cores with a 10% polydispersity. The refractive index for the anatase core is taken as 2.3, for the nondried titania shells as 1.55, for the dried titania shells as 1.8, and for the titania-silica composite shell as 1.55 (k = scattering vector).

without the silica. It was also observed that the incorporation of silica into the amorphous titania shell prevents particle shrinkage as a result of drying. Note that the absence of the shrinkage also contributes to a lower index of the final shells. For comparison, the nondried shell was 300 nm (curve 3), and it shrank to 130 nm (curve 1) if silica was not added. However, its thickness was sustained at 290 nm after incorporation of silica as seen in curve (2) of Figure 4a. The size difference for the dried titania and the dried composite shell were also supported by the TEM analysis (Table 1). Furthermore, if the anatase core, titania−silica composite shell particles are calcined in an oven at 500 °C, the core will remain anatase with the same refractive index; however, the shell refractive index will increase due to the crystallization of the titania there.

The amount of silica incorporated into the shell is tunable by the amount of silica added and changed the refractive index of the shell. To investigate this, we prepared two samples with different silica content and calcined them at 500 °C for 1 h. These particles were then dispersed in ethanol and examined with SLS. The indices of refraction for these particles were found to be 1.6 (0.2 mL of TEOS for shells made with 0.15 mL of TBT) and 1.7 (0.1 mL of TEOS for 0.14 mL of TBT) for (1) and (2), respectively, in Figure 4b. To observe higher indices the silica content (but using APS as a silica precursor) was decreased. Two new batches were prepared containing 2 and 10 μL of APS for shells made with 0.065 mL of TBT. These batches were calcined at 450 °C for 2 h. The indices of refraction for these particles were found to be 2.05 and 2.0 for (1) and (2), respectively, in Figure 4c. On the basis of these observations we conclude that by changing the silica content one can tailor the refractive index of the composite shell from 1.55 to 2.3.

The microstructure of the particles was also investigated by means of TEM. Figure 5a shows a TEM image of anatase−titania cores. Figure 5b is a TEM image of core−shell particles with an anatase core and an amorphous−titania shell. Figure 5c shows a TEM image of a broken core−shell particle after application of mechanical force. The sphericity of the titania particles was preserved, and the polydispersity decreased by seeded growth of the particles. We have also imaged the particles with a titania−silica composite shell. Figure 6a shows an image of anatase core−titania−silica composite shell particles (same particles as in Figure 4a(2)). Note that the core−shell structure is clearly visible in the TEM image, whereas this was less the case for anatase core, titania shell particles (Figure 5b). This difference is due to the density decrease in the composite shell by addition of silica and the shrinkage of the pure titania shell due to the electron beam. A lower-density shell increases the contrast between the core and the shell. To prove that silica and titania coexist in the shell and that the core is much denser because of the crystallinity, we performed an energy dispersive X-ray spectroscopy (EDX) analysis of the particles shown in Figure 6a. It can be seen from the EDX line scan given in Figure 6b that the shell has a composite structure because in the shell both silica and titania peaks exist. The titania signal in the middle of the line scan increases proving that the crystalline titania core was denser than the shell. The silica

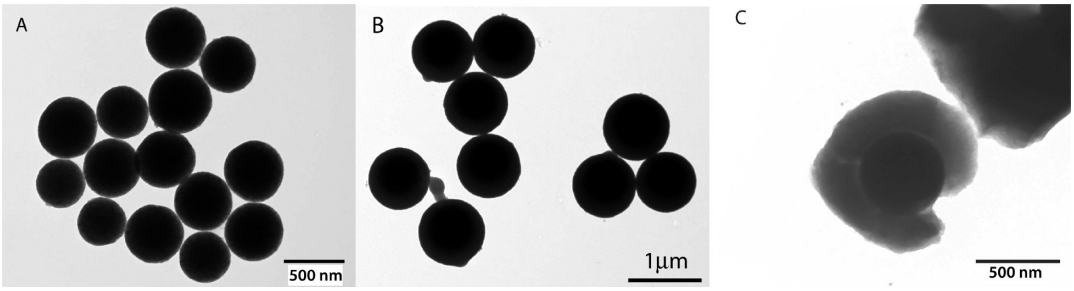

Figure 5. TEM images of (a) anatase core particles with a size of 450 nm and 10% polydispersity (b) core−shell particles of which the SLS curve is given in Figure 2d, with a size of 970 nm in diameter, and (c) a crushed core−shell particle after application of a mechanical force, which clearly shows the core−shell structure of the system.

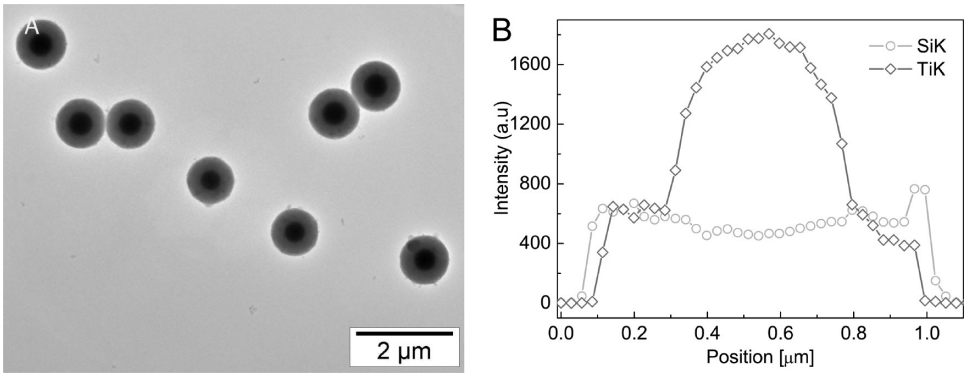

Figure 6. (a) TEM image of anatase core−composite titania−silica shell particles SLS data shown in Figure 4a(2). (b) EDX line scans of Si−K and Ti−K lines through an anatase core, with the composite titania−silica shell particle given in a.

signal exists on the shell and decreases in the middle of the line scan, which is consistent with silica being present only in the shell and not in the core of the sphere.

It was shown recently, that APS incorporated in silica resulted in luminescence after calcination between 450 and 700 °C.[30,31] The residues of APS (NH-related groups[37] and oxygen-related defects[38]) were thought to cause the luminescence in the oxide matrix. The exact origin of the luminescence is not understood well, yet. However, it was shown that amino−containing precursors had a higher intensity compared to other precursors that only contained hydrocarbons.[31] It was also shown that C−O vibrations were responsible for the luminescence in the silica matrix.[38] On this basis, we think that the luminescence mechanism in silica involves C−O related defect centers. Additionally, NH-groups enhance the luminescence with electron-donating ability[39] because this luminescence is a result of electron−hole recombination. The recombination mechanism results in the dependence of emission wavelength on the excitation wavelength.[39] It is expected that, if the high energy band gap of silica (5.4 eV[39]) can be decreased by addition of impurities, the comparably lower band gap of titania (3.0 eV[40]) can also be decreased, that is, it can interact with visible light.

To observe the effect of APS impurities in titania, we incorporated APS into the shell of anatase−titania particles by simply adding APS and NH_3 to the as-synthesized particles, prior to drying. We have observed, similar to silica, that this doping of the titania matrix also results in luminescence after calcination at 400−450 °C. Three samples were prepared with 0.5, 2, and 10 μL of APS for shells made with 0.065 mL of TBT.

We first observed the luminescence by illuminating the particles with a mercury lamp equipped with filter cubes on a confocal microscopy stage. When illuminated by blue light (420−490 nm) the particles luminesced yellow-orange, and when illuminated by green (515−560 nm) they luminesced red. The confocal microscopy image in Figure 7a shows particles doped with 2 μL of APS. The particles were illuminated with a 488 nm laser, and the detection was made in the range of 590−620 nm. The core−shell structure is immediately apparent as the luminescence originates only from the shell where the APS is incorporated. Figure 7b shows the fluorescence spectra of these particles with an excitation wavelength of 390 nm. The fluorescence intensity is decreased as the APS concentration increased, similarly to the silica system.[31] To test whether this luminescence could also be excited by visible light, we looked at the luminescence while exciting with 470 nm (Figure 7c). The decrease in the fluorescence intensity, as the APS concentration increased, was observed here as well. The broad fluorescence peak of the 0.5 μL APS sample at 610 nm corresponds to yellow-orange which coincides with our observations. As the concentration of APS increased the peak shifted to red, fluorescence intensity was the highest for the lowest concentration of APS. We decreased the concentration of APS to 0.15 μL and observed that the intensity was high and particles luminesce yellow under blue illumination. For comparison we mixed these particles with FITC labeled silica particles (0.2%(m/m) FITC per SiO_2). Figure 7d shows intensity profiles of a confocal microscopy image (inset) of a silica (green) and a titania (red) particle of the batch to which

(37) Carlos, L. D.; Ferreira, R. A. S.; Pereira, R. N.; Assuncao, M.; Bermudez, V. D. *J. Phys. Chem. B* **2004**, *108*, 14924–14932.
(38) Green, W. H.; Le, K. P.; Grey, J.; Au, T. T.; Sailor, M. J. *Science* **1997**, *276*, 1826–1828.
(39) Brankova, T.; Bekiari, V.; Lianos, P. *Chem. Mater.* **2003**, *15*, 1855–1859.
(40) Umebayashi, T.; Yamaki, T.; Itoh, H.; Asai, K. *Appl. Phys. Lett.* **2002**, *81*, 454–456.

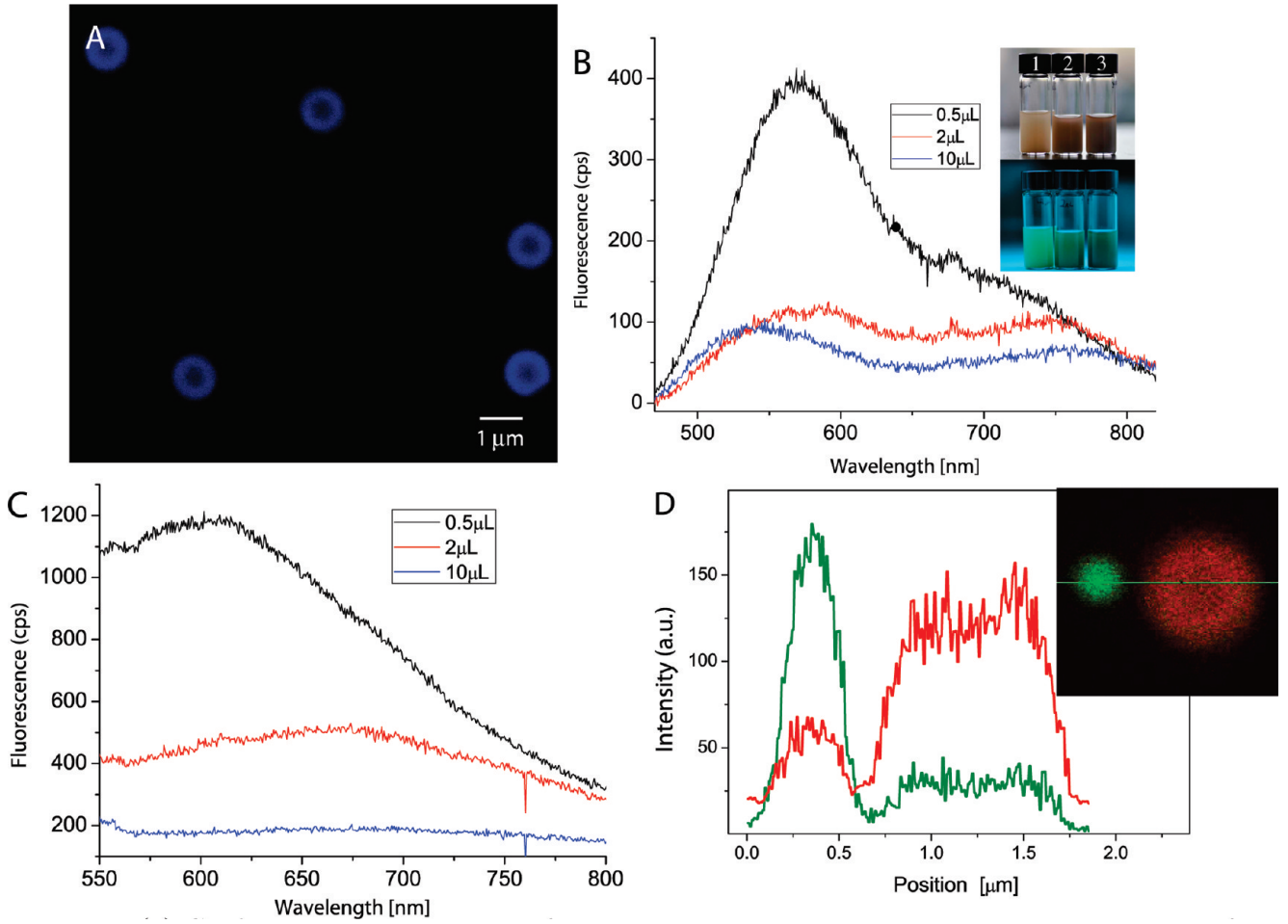

Figure 7. (a) Confocal microscopy image of titania particles made luminescent by incorporation of APS. SLS data of these particles are shown in Figure 4c(1) (2 μL of APS). The excitation was 488 nm, and the detection band is between 590 and 620 nm for the confocal microscopy image. (b) Fluorescence spectra of the particles excited with 390 nm. Inset shows the photos of the particles illuminated with day light (above) and UV light (below) with APS amounts of 0.5, 2, and 10 μL, respectively. (c) Fluorescence spectra of the particles excited with 470 nm. (d) Intensity profile of the confocal image shown in the inset on the line shown, green (small) is a FITC labeled silica particle, and red (large) is an APS incorporated titania particle with 0.5 μL APS for shells made with 0.065 mL of TBT.

0.5 μL of APS was added. The particles were excited with a 488 nm laser and imaged with 515/30 (FITC) and 605/75 (APS-titania) detectors. As can be seen from the image and profile, the fluorescence of the titania particles were comparable to the FITC labeled particles (see Supporting Information, Figure S3 for a confocal image.) This luminescence of titania was observed at room temperature, contrary to the previous literature which demonstrated luminescence at low temperatures only.[26,41] In addition, this is an easy and cost-effective way of labeling particles and may also attract attention for use in other applications of luminescent titania in photonic crystals, where often a high temperature step is taken. Furthermore, the labeling of titania by this method can be made possible at elevated temperatures (for example, when chemical vapor deposition is utilized), which is impossible with organic dyes of which the fluorescence degrades or which simply burns up.

4. Conclusions

We reported a way of coating anatase particles with amorphous titania yielding monodisperse core−shell spheres without the use of a glovebox or a nitrogen environment. This is also one of the first examples of seeded growth shown for titania-on-titania. The method allows coating of a thick layer of titania in one step, which can significantly decrease the polydispersity. We have also shown that, by manipulating the amorphous titania shell by incorporation of silica into the pores after the synthesis, it is possible to tailor the refractive index of the amorphous shell. In principle, the manipulation of the refractive index can also be done for particles with no core−shell structure. Finally, we have shown that the addition of APS followed by calcination causes luminescence of the titania particles at room temperature without the addition of any fluorophore to the system comparable in level to that of laser dyes. This method opens the possibility to develop photonic crystal applications due to the monodispersity and the high refractive index of the particle, which also offers the possibility to manipulate core and shell separately. Monodisperse titania particles with a high refractive index core and low−index shell can be useful for optical tweezing of high refractive index particles. Bormuth et al.[19] and Jannasch et al.[20] have shown that coated microspheres where the coating works as a kind of "antireflection" coating can reduce the scattering forces and lead to stronger trapping in optical tweezing. The use of antireflection-coated titania particles for optical trapping can reduce photodamage in sensitive biophysical assays or increase the maximum force achievable

(41) Watanabe, M.; Sasaki, S.; Hayashi, T. *J. Lumin.* **2000**, *87−89*, 1234–1236.

with optical tweezers. Nanonewton light forces seem feasible, which opens up new experimental possibilities for force spectroscopy with the exquisite force resolution of optical tweezers.

Acknowledgment. We thank J. D. Meeldijk (Electron Microscopy Utrecht) for the assistance with the EDX measurements. Yiming Zhao and Andries Meijerink (Utrecht University, Condensed Matter and Interfaces) are acknowledged for spectrofluorometry measurements and discussions.

Supporting Information Available: SLS curves for the titania particles studied by means of digital holographic microscopy (Figure S1), diameter from TEM and SLS of the particles in Figure S1 (Table S1), SLS experimental curves of the titania particles fitted to different theoretical calculations (Figure S2), and confocal fluorescence microscopy image of a mixture of FITC labeled silica particles and APS incorporated and calcined titania particles (Figure S3). This material is available free of charge via the Internet at http://pubs.acs.org.